Voltage-Dependent Sodium Channel Function Is Regulated Through Membrane Mechanics

Anatoly Shcherbatko,* Fumihito Ono,* Gail Mandel,*# and Paul Brehm*

*Department of Neurobiology and Behavior and #Howard Hughes Medical Institute, State University of New York at Stony Brook, Stony Brook, New York 11794 USA

ABSTRACT   Cut-open recordings from *Xenopus* oocytes expressing either nerve (PN1) or skeletal muscle (SkM1) Na^+ channel α subunits revealed slow inactivation onset and recovery kinetics of inward current. In contrast, recordings using the macropatch configuration resulted in an immediate negative shift in the voltage-dependence of inactivation and activation, as well as time-dependent shifts in kinetics when compared to cut-open recordings. Specifically, a slow transition from predominantly slow onset and recovery to exclusively fast onset and fast recovery from inactivation occurred. The shift to fast inactivation was accelerated by patch excision and by agents that disrupted microtubule formation. Application of positive pressure to cell-attached macropatch electrodes prevented the shift in kinetics, while negative pressure led to an abrupt shift to fast inactivation. Simultaneous electrophysiological recording and video imaging of the cell-attached patch membrane revealed that the pressure-induced shift to fast inactivation coincided with rupture of sites of membrane attachment to cytoskeleton. These findings raise the possibility that the negative shift in voltage-dependence and the fast kinetics observed normally for endogenous Na^+ channels involve mechanical destabilization. Our observation that the $\beta1$ subunit causes similar changes in function of the Na^+ channel α subunit suggests that $\beta1$ may act through interaction with cytoskeleton.

INTRODUCTION

Voltage-gated Na^+ channels are heteromeric complexes consisting of a large pore-forming α subunit and one or more small auxiliary β subunits (Hartshorne and Catterall, 1984). Mammalian brain Na^+ channels are complexes of α (260 kD) and two distinct auxiliary subunits designated $\beta1$ (23 kD) and $\beta2$ (21 kD). Skeletal muscle Na^+ channels are heterodimers composed of an α subunit and a single β subunit (38 kD), which is homologous to the brain $\beta1$ subunit (Isom et al., 1994). Expression of rat brain or rat skeletal muscle Na^+ channel α subunits alone in *Xenopus* oocytes yields Na^+ currents that activate and inactivate in response to depolarization and are inhibited by TTX (Goldin et al., 1986; Trimmer et al., 1989; Joho et al., 1990). However, as first reported by Auld et al. (1988), Na^+ currents resulting from injection of α subunit RNA inactivate more slowly than channels present in endogenous tissue. Rapid inactivation of Na^+ current is restored when α subunits are coexpressed with low molecular weight rat brain mRNA, suggesting a possible requirement for auxiliary subunits for normal functional expression (Auld et al., 1988; Krafte et al., 1990). Indeed, coexpression of rat brain $\beta1$ subunit RNA with type IIA α RNA results in accelerated inactivation of Na^+ current, increased peak current amplitude, and shifts in the voltage-dependence of inactivation to more negative membrane potentials. These changes all mimic the effects of low molecular weight brain mRNA on Na^+ channel expression and function (Isom et al., 1992).

The existence of factors other than auxiliary β subunits that can alter inactivation kinetics has been suggested by studies in which Na^+ channel α subunits are expressed in cells lacking endogenous Na^+ channel α and $\beta1$ subunits. Expression of rat cardiac (rH1) and rat brain type IIA in mammalian cell lines results in Na^+ channels with rapid activation and inactivation characteristic of native neuronal Na^+ channels (Scheuer et al., 1990; West et al., 1992; Qu et al., 1994). Similar results have been obtained after transient expression of the rat and human skeletal muscle SkM1 Na^+ channels in human embryonic kidney (HEK 293) cells (Ukomadu et al., 1992; Chahine et al., 1994).

The mechanisms governing fast and slow inactivation of Na^+ channels are poorly understood. A growing body of evidence supports the hypothesis that fast and slow inactivation are structurally distinct processes that are not tightly coupled and are not mutually exclusive (Rudy, 1978; Featherstone et al., 1996; Townsend and Horn, 1997; Vedantham and Cannon, 1998). Single-channel analysis of rat brain (Moorman et al., 1990) and skeletal muscle (Zhou et al., 1991) Na^+ channel α subunits, expressed in *Xenopus* oocytes, show interconversion between two inactivation modes. Thus, the α subunit does not have an absolute requirement for the auxiliary subunits in order to exhibit normal gating behavior. Consistent with this idea, several studies have identified conditions under which exogenously expressed α subunits can be converted from slow to fast inactivation without the aid of a $\beta1$ subunit (Krafte et al., 1990; Zhou et al., 1991; Fahlke and Rudel, 1992; Fleig et al., 1994; Chen and Cannon, 1995). The results presented in this paper extend these observations by showing conversion of α subunit from slow to exclusively fast inactivation

through cytoskeletal disruption. The functional characteristics of the converted α subunit are quantitatively similar to the actions of the $\beta1$ subunit, suggesting a common mechanism.

METHODS

Sections of ovary were surgically isolated from anesthetized *Xenopus* frogs (Nasco, Fort Atkinson, WI) and were enzymatically treated with 10 mg/ml collagenase (Gibco BRL, Grand Island, NY) for 20 min. After extensive washing the follicle cell layer was mechanically removed from stage V-VI oocytes and cells were allowed to recover in a nutrient OR-3 medium overnight. The OR-3 medium contained 50% L-15 medium, 100 μg/ml gentamycin, 4 mM glutamine, and 30 mM Na-HEPES (all Gibco BRL, Grand Island, NY), pH-adjusted to 7.6 with NaOH. The next day, oocytes were individually injected with 100–140 ng of RNA coding for either SkM1 (Trimmer et al., 1989) or human PN1 (Klugbauer et al., 1995, kindly provided by F. Hoffman) α subunit. In cases where human $\beta1$ (Makita et al., 1994, kindly provided by A. George) was tested, the oocytes were injected with a mixture of 75 ng α RNA and 25 ng $\beta1$ RNA, and maintained at 18°C in OR-3 medium. The methods used to synthesize the RNA were identical to those previously published (Murray et al., 1995).

Na$^+$ current was measured using either standard cut-open oocyte voltage clamp (Taglialatela et al., 1992) or macropatch techniques (Leonard et al., 1986) within 2–5 days after the RNA injection. In both cases the current was generally recorded from the animal side of the oocyte at 21–22°C. For micropatch and macropatch recordings, the oocytes' vitelline membrane was removed manually and the oocyte was repeatedly penetrated with a blunt electrode. This action, combined with the high-potassium bath solution, nulled the membrane potential. The bath solution contained (in mM): 120 KCH$_3$SO$_3$, 2 MgCl$_2$, 1 K-EGTA, and 10 K-HEPES at pH 7.2. Micropatch electrodes were pulled to a final outer diameter (O.D.) of ~2–5 μm using a Flaming/Brown micropipette puller (Model P97, Sutter Instrument Co., Novato, CA) and lightly fire-polished. Macropatch pipettes (borosilicate glass, WPI, Sarasota, FL) were pulled to an O.D. of ~20 μm, coated with a 1:3 mixture of Parafilm/mineral oil, and fire-polished to a final tip diameter of ~10–15 μm. Pipettes were filled with a solution containing (in mM): 120 NaCH$_3$SO$_3$, 2 CaCl$_2$, and 10 Na-HEPES at pH 7.2. Both cell-attached and excised patches formed seals in excess of 2 GΩ upon application of steady, gentle, negative pressure. Na$^+$ currents were recorded by means of an Axopatch 200A amplifier (Axon Instruments, Inc., Burlingame, CA) and processed using HEKA Pulse software (Instrutech, Great Neck, NY). The currents were sampled at 50 kHz and filtered at 10 kHz before analysis. Capacitive transients were compensated using a combination of manual compensation on the amplifier and further processing using either a P/4 or P/10 leak subtraction protocol.

For cut-open oocyte voltage clamp recordings the three-compartment chamber provided with the CA-1 voltage clamp (Dagan Corporation, Minneapolis, MN) was used. Both top and guard chamber solution contained (in mM): 110 NaCH$_3$SO$_3$, 2Ca(CH$_3$SO$_3$)$_2$, and 10 Na-HEPES at pH 7.2. The bottom chamber contiguous with the cell interior contained a solution composed of (in mM): 120 KCH$_3$SO$_3$, 1 K-EGTA, and 10 K-HEPES at pH 7.2. Agar bridges filled with 120 mM NaCH$_3$SO$_3$ and containing a black platinized platinum wire were used to pass current and control the chamber potentials. An intracellular micropipette filled with 3 M KCl (~100 kΩ) measured the membrane potential. Currents were acquired using a CA-1 oocyte clamp amplifier (Dagan). Oocytes that showed an obvious lack of proper voltage control were discarded.

Data analysis was performed using HEKA PulseFit software (Instrutech, Great Neck, NY) and IGOR Pro (WaveMetrics, Lake Oswego, OR). The current-voltage relationships for Na$^+$ currents were fitted by the Goldman-Hodgkin-Katz equations and the half-activation potential was determined on the basis of the fit. Steady-state inactivation data were fitted with a Boltzmann equation $I(V) = $ amplitude/$(1 + \exp(-(V - V_{half})/$ slope$))$ and midpoint of inactivation determined from this relationship. The decay of Na$^+$ currents and time course of recovery from inactivation were fitted by either single or summed exponential functions. Cumulative data are presented as the means and standard deviations (means ± SD).

Video imaging of the macropatch was performed on a Zeiss Axioscope FS-2 using a 63× water-immersion Zeiss physiology objective (n.a. 0.9) with further magnification provided by a 2× optovar. Differential interference contrast provided a sharp image of the plasma membrane of the oocyte and the pigmented cytoplasmic inclusions located at the animal pole. Video of the entire experimental sequence was performed using a Sony RGB color video camera (model DXC-960MD). The video images were acquired at rates of either 0.2 Hz or 0.5 Hz with a Scion Instruments LG-3 frame-grabber by means of a Power Macintosh G3 computer. The stored video images were processed off-line using National Institutes of Health image software. Electrophysiological recording of the macropatch Na$^+$ current in response to a 10 ms depolarization to −10 mV was synchronized to video acquisition. Accordingly, the corresponding video frame and Na$^+$ current could be matched for analysis. Intrapipette pressure was controlled using a pneumatic transducer tester DPM-IB (Bio-Tek Instruments, Winooski, VT).

RESULTS

Coexpression of the $\beta1$ subunit alters Na$^+$ channel α subunit function

Cut-open oocyte voltage clamp recordings were used to compare the functional properties Na$^+$ channel α subunits to $\alpha + \beta1$ channels. The Na$^+$ current resulting from expression of either PN1 (Fig. 1 *A*) or SkM1 (Fig. 2 *A*) α subunits alone exhibited a slow decay of inward current, reflecting slow channel inactivation. The majority of SkM1 and PN1 α subunit patches exhibited a pure monoexponential decay of inward current. For SkM1 channels, inactivation occurred with an average time constant of 14 ± 4 ms ($n = 10$) at a membrane potential of −5 mV. Slightly faster rates of inactivation were observed for PN1 α subunits, which averaged 9 ± 3 ms ($n = 9$) at 5 mV. Coinjection of the $\beta1$ subunit RNA with either PN1 (Fig. 1 *B*) or SkM1 (Fig. 2 *B*) α subunit RNA in *Xenopus* oocytes resulted in fast inactivation of Na$^+$ current. The time course of current decay was monoexponential with a fitted time constant corresponding to 1.3 ± 0.2 ms ($n = 6$) at −5 mV for PN1 and 0.9 ± 0.1 ms ($n = 11$) at −10 mV for SkM1 Na$^+$ channels.

The effects of $\beta1$ subunits on the voltage-dependence of activation and inactivation were determined for both PN1 and SkM1 Na$^+$ channel types. Comparisons of the current-voltage relations indicated that $\beta1$ left-shifted the midpoint of activation by an average of −6 mV for PN1 (Fig. 1 *C*) and −5 mV for SkM1 (Fig. 2 *C*). Steady-state inactivation was determined by use of either a 300-ms (for PN1) or 800-ms (for SkM1) conditioning pulse to produce inactivation followed by a 10-ms test pulse to a voltage corresponding to peak inward current. These parameters were selected because they consistently produced a steady-state level of inactivation for each channel isoform. Boltzmann fits to the steady-state inactivation relations obtained from PN1 Na$^+$ channels indicated no difference in the midpoint for α and $\alpha + \beta1$ channels (Fig. 1 *D*). Fitting of the SkM1 relations indicated a −6 mV shift in steady-state inactivation for $\alpha + \beta1$ channels (Fig. 2 *D*).

Fast inactivation of inward current could also be experimentally induced by "super-injection" of RNA. Pure slow inactivation of both PN1 and SkM1 Na$^+$ channel α subunits
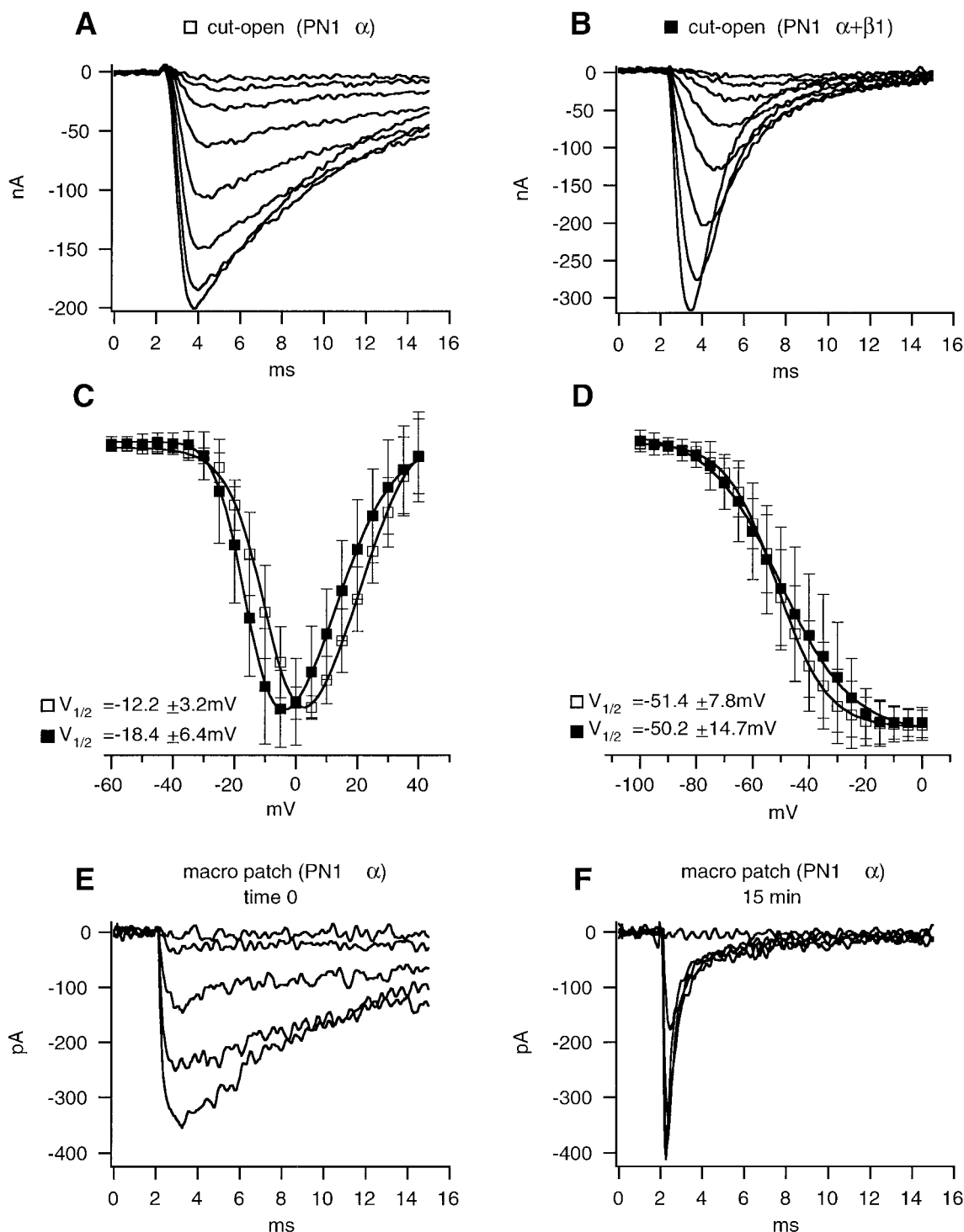
FIGURE 1 Effects of coexpression of the $\beta 1$ subunit and cell-attached macropatch recording on PN1 α subunit function. (*A*) Cut-open voltage clamp recordings of Na^+ currents from *Xenopus* oocytes expressing α subunit alone and (*B*) expressing both α and $\beta 1$ subunits. In both oocytes the voltage was stepped from a holding potential of -100 mV in increments of 5 mV, starting from -30 mV for *A* and -40 mV for *B*. (*C*) Normalized current-voltage relationship of PN1 Na^+ channels formed by the α subunit alone (*open squares, n = 9* oocytes) and by α and $\beta 1$ subunits (*closed squares, n = 7*). (*D*) Steady-state inactivation of Na^+ channels formed from the α subunit alone (*open squares, n = 6*) and by α and $\beta 1$ subunits (*closed squares, n = 9*). Oocytes were held at -100 mV and depolarized, every 10 s, with a 300-ms conditioning pulse to produce inactivation. The peak current amplitude measured during a test pulse to 0 mV was normalized to the maximum current amplitude and is plotted as a function of the conditioning pulse potential. Both data sets were fit using the Boltzmann function yielding the indicated $V_{1/2}$ values. (*E*) Cell-attached macropatch recordings from the oocyte expressing the PN1 α subunit alone immediately following seal formation. The membrane potential was stepped from -140 mV to potentials between -50 mV and -10 mV in 10-mV increments at 3-s intervals. (*F*) Cell-attached macropatch recordings from the same oocyte 15 min after formation of the seal. The membrane potential was stepped from -140 mV to potentials between -50 mV and -10 mV in 10-mV increments at 3-s intervals.
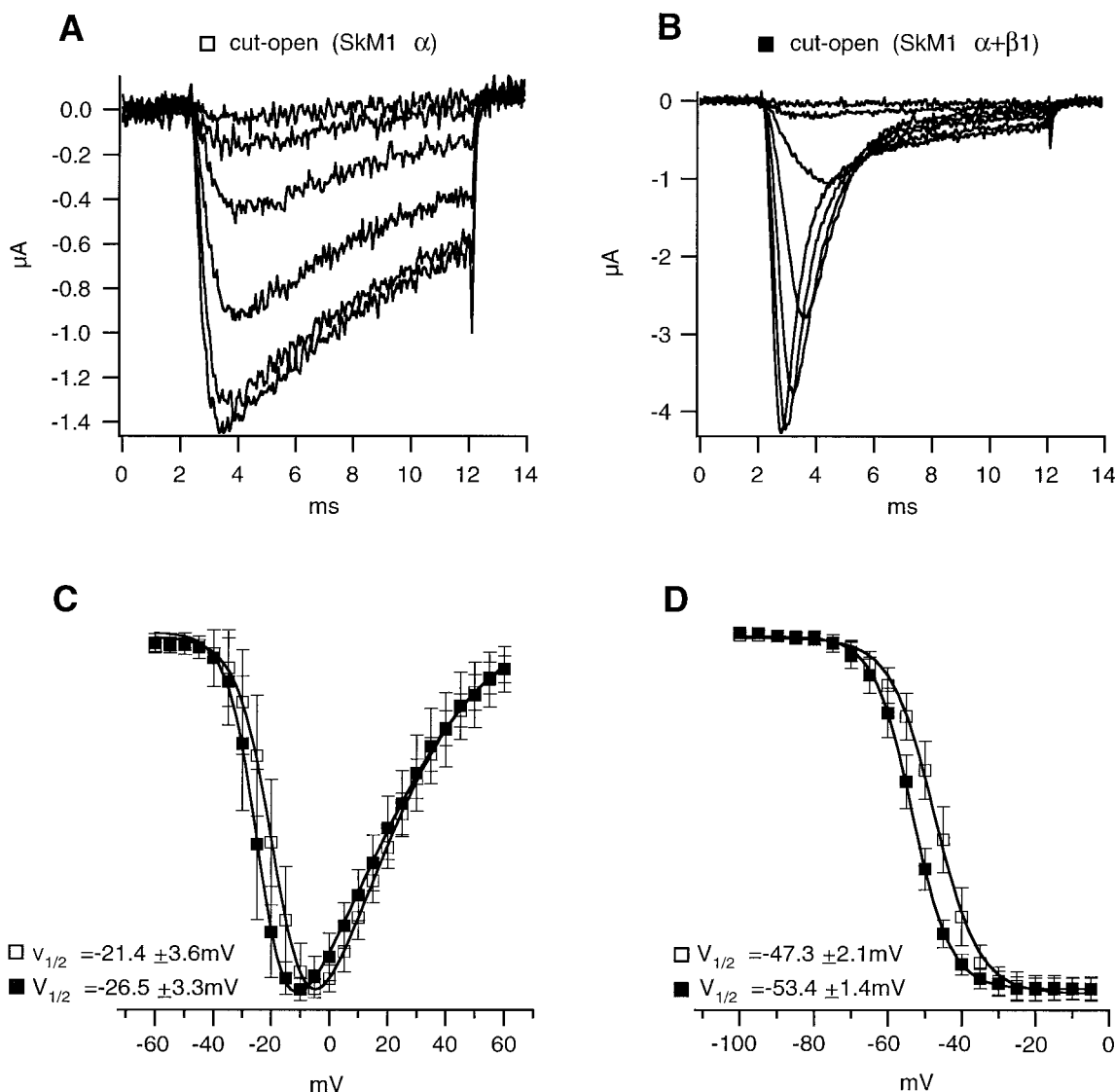
FIGURE 2   Effects of coexpression of the $\beta 1$ subunit on SkM1 α subunit function. (*A*) Cut-open voltage clamp recordings of Na$^+$ currents from *Xenopus* oocytes expressing the α subunit alone and (*B*) expressing both α and $\beta 1$ subunits. In both oocytes the voltage was stepped from a holding potential of -140 mV in increments of 5 mV, starting from -30 mV for *A* and -40 mV for *B*. (*C*) Normalized current-voltage relationship of PN1 Na$^+$ channels formed by the α subunit alone (*open squares, n* = 10 oocytes) and by α and $\beta 1$ subunits (*closed squares, n* = 11). (*D*) Steady-state inactivation of Na$^+$ channels formed from the α subunit alone (*open squares, n* = 10) and by α and $\beta 1$ subunits (*closed squares, n* = 11). Oocytes were held at -140 mV and depolarized, every 10 s, with an 800-ms conditioning pulse to produce inactivation. The peak current amplitude measured during a test pulse to -5 mV was normalized to the maximum current amplitude and was plotted as a function of the conditioning pulse potential. Both data sets were fit using the Boltzmann function yielding the indicated $V_{1/2}$ values.

was faithfully observed under conditions wherein ~ 100 ng of α subunit RNA was injected into the oocyte. By contrast, injection of ~ 1.5 μg of α subunit RNA encoding either channel type resulted in currents that decayed with a biphasic time course. In the case of SkM1 α subunits the fast component of inactivation accounted for over half of the total inward current (data not shown) and had an average time constant of 0.5 ± 0.2 ms (n = 5) at -10 mV. The residual slowly inactivating inward current decayed with the typical slow time constants observed for pure slow currents. Neither the voltage-dependence of inactivation nor activation was shifted as a result of the fast inactivation, indicating

that the fast and slow components of inactivation had similar voltage-dependence. The possibility that the fast inactivation represented a loss of voltage control due to the large size of the current ($20-50$ μA) was ruled out by reducing external sodium concentration. Reduction of Na$^+$ current did not affect the biexponential decay of inward current.

Macropatch recording alters voltage-dependence and kinetics of α subunit function

In the cut-open mode of voltage clamp the Na$^+$ current associated with the α subunit was stable over time ($>$30

min) without any noticeable change in amplitude or kinetics ($n = 30$) (Fig. 3 *A*). However, formation of large cell-attached patches using the macropatch configuration (pipette tip O.D. ~15 μm) consistently resulted in a gradual and permanent transition to fast inactivation over the course of minutes ($n = 40$). Immediately after formation of the macropatch (Figs. 1 *E* and 3 *B*) the time course of inactivation of Na$^+$ current was indistinguishable from that obtained using the cut-open recordings from the same oocyte (Figs. 1 *A* and 3 *A*). However, over time, a fast component of inactivation appeared that resulted in an overall decay that was described by a biexponential function (Figs. 1 *F* and 3 *C*). This transition was not accompanied by any substantial change in peak inward current (Fig. 3, *B* and *C*). Furthermore, measurement of the amplitudes of fast and slow inactivating components indicated a slow transition to pure fast inactivation with no change in overall current amplitude (Fig. 3 *F*). In a few experiments the macropatch was intentionally excised from the oocyte by drawing the patch pipette far away from the cell. In all of these cases the transition to fast inactivation was accelerated.

The macropatch recordings also revealed differences in voltage-dependence compared to recordings obtained using the cut-open voltage clamp technique. Large negative shifts in the current-voltage relations (Fig. 3 *D*) and steady-state inactivation (Fig. 3 *E*) were observed immediately after seal formation. A smaller left shift in voltage-dependence of both activation and inactivation occured during the subsequent 15 min of recording. This difference in voltage-dependence was not due to errors in estimating the actual membrane potential for macropatch recording because the oocyte membrane was pierced by a blunt electrode in the presence of 120 mM KCH$_3$SO$_3$ to fully eliminate the resting potential. The midpoint of activation for cut-open recordings averaged -21.4 ± 3.6 mV ($n = 9$) compared to -44.7 ± 3.3 mV ($n = 9$) for macropatch recordings (Fig. 3 *D*). This represented a 23 mV difference in the voltage-dependence of activation. The midpoint of steady-state inactivation for cut-open recordings averaged -47.3 ± 2.1 mV ($n = 9$) compared to -92.9 ± 7.3 mV ($n = 9$) for macropatch recordings (Fig. 3 *E*). This represented a 46 mV difference in the voltage-dependence of inactivation.

Comparison of β1 subunit effects on channel function to the macropatch-induced changes in function

The effect of macropatch recording on Na$^+$ channel inactivation kinetics (Figs. 3, *B* and *C*; 4 *C*) appears to be qualitatively similar to the effects mediated by β1 subunit coexpression (Fig. 4). Unlike the time-dependent transition to fast inactivation kinetics by α subunits alone, macropatches from oocytes expressing both α and β1 subunits exhibited fast inactivation from the onset of seal formation. Quantitative differences of these two mediators of fast inactivation were examined by measuring the voltage-depen-

dence of fast inactivation time constants for cut-open $\alpha+\beta$1, macropatch $\alpha+\beta$1, and macropatch α Na$^+$ current after the time-dependent shift to fast inactivation. No significant differences were measured for macropatch $\alpha+\beta$1 versus macropatch α currents after transition to pure fast inactivation (Fig. 4 *F*). Thus, β1 subunits have no additive effect on speeding inactivation beyond that observed for the α subunit alone. Further comparisons to cut-open recordings were complicated by the macropatch-induced change in the voltage-dependence. However, it appears that differences in the time constants of fast inactivation exist between cut-open $\alpha+\beta$1 and macropatch α Na$^+$ current (Fig. 4 *F*). In particular, the inactivation time constants for cut-open $\alpha+\beta$1 current are larger at all potentials tested. Due to the differences in voltage-dependence it is not possible to precisely compare time constants at negative potentials: the range over which inactivation kinetics are highly voltage-dependent. However, comparisons at positive potentials reveal a small difference. An explanation for these differences may reside in the effects of macropatch formation on acceleration of activation kinetics, a point which will be discussed in a later section.

Similar actions of β1 and macropatch formation on α subunit function are reflected in the recovery rates for fast and slow inactivating components of inward current. Recovery rates from inactivation were determined using 800-ms inactivating prepulses to -10 mV, followed by a test pulse at prescribed recovery intervals (Fig. 5 *A*). Overall results from five oocytes expressing SkM1 α subunits indicated that Na$^+$ current recovery follows a biexponential time course at -140 mV. Moreover, the two time-dependent components of recovery correspond to fast and slow inactivating components of inward current, respectively. This is reflected in the measurements of the individual contribution of fast and slowly decaying inward currents to the overall inward current at each interval. For interpulse intervals <10 ms the inactivation of pulse 2 inward current was purely fast, with a time constant corresponding to 0.7 ms (Fig. 5 *A*). This fast inactivation contrasted with the observed decay of pulse 1 current which, in all trials, exhibited >90% slow inactivation. At longer interpulse intervals the recovered current exhibited mixed slow and fast inactivation with progressively greater contribution by slow inactivation with increased recovery interval. By the time that the interval reached 0.5 s the current was predominantly slowly inactivating, as demonstrated by the pulse 2 current trajectory (Fig. 5 *A*).

The time constants for recovery of fast inactivating components of the SkM1 α subunit measured by the cut-open recording technique (Fig. 5 *B*) were compared to those measured for fast inactivating currents seen in the presence of β1 subunit (Fig. 5 *D*) and after macropatch conversion of α subunit (Fig. 5 *C*). Comparisons of the recovery curves for cut-open recordings of SkM1 $\alpha+\beta$1 currents to those obtained after macropatch-induced conversion of SkM1 α subunit showed similar fast time constants for recovery. These data support the idea that the β1 subunit acts to speed
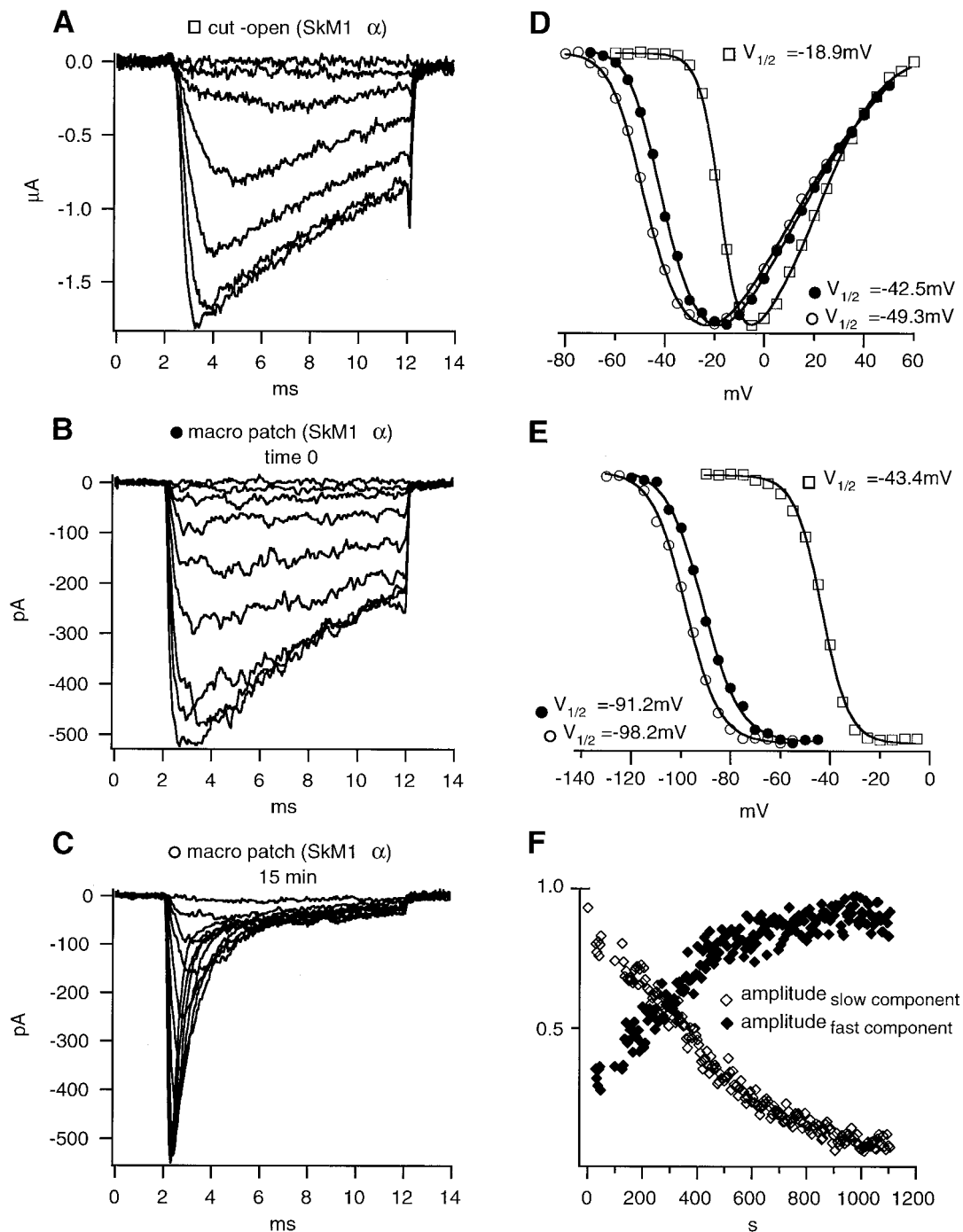
FIGURE 3   Effect of cell-attached macropatch recording on the functional properties of the SkM1 α subunit. (A) Cut-open voltage clamp recordings of Na^+ currents from *Xenopus* oocytes expressing α subunit alone. The membrane potential was stepped from -140 mV to potentials between -35 mV and -5 mV in 5-mV increments at 3-s intervals. (B) Cell-attached macropatch recordings from the same oocyte shown in A immediately after seal formation. The membrane potential was stepped from -140 mV to potentials between -60 mV and -20 mV in 5-mV increments at 3-s intervals. (C) Cell-attached macropatch recordings from the same oocyte 15 min after formation of the seal. The membrane potential was stepped from -140 mV to potentials between -70 mV and -20 mV in 5-mV increments at 3-s intervals. (D) Current-voltage relationships for peak Na^+ currents recorded by cut-open voltage clamp (*open squares*) cell-attached macropatch configuration immediately after seal formation (*closed circles*) and 15 min subsequent to seal formation (*open circles*). (E) Steady-state inactivation curves for Na^+ current recorded by cut-open voltage clamp (*open squares*), cell-attached macropatch configuration immediately after seal formation (*closed circles*) and 15 min subsequent to seal formation (*open circles*). Oocyte was held at -140 mV and depolarized, every 5 s, with an 800-ms conditioning pulse to produce inactivation. The peak current amplitude measured during a test pulse to the potential corresponding to peak inward current in D was normalized to the maximum current amplitude and is plotted as a function of the conditioning pulse potential. Both data sets were fit using Boltzmann function yielding the indicated $V_{1/2}$ values. (F) Time-dependent changes in the relative proportions of slow (*open symbols*) and fast (*closed symbols*) inactivating Na^+ current during macropatch recording. Na^+ currents were evoked by voltage step to -20 mV from a holding potential of -140 mV. The decay of inward current was fitted with a double exponential function and corresponding peak amplitudes of fast and slow components were estimated on the basis of the fitted curves.
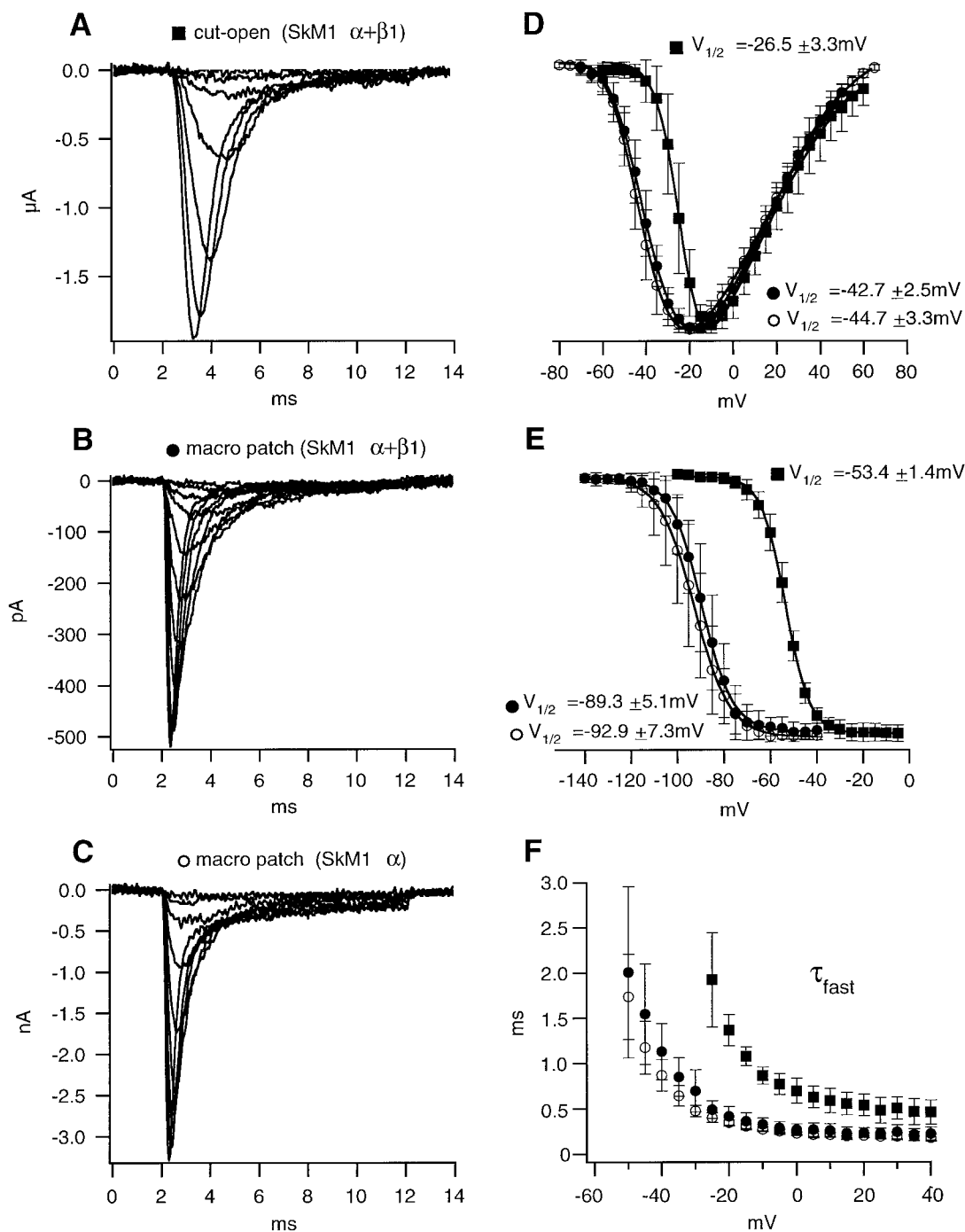
FIGURE 4   Comparisons of $\beta1$ subunit and macropatch-induced conversion of the α subunit function. (*A*) Cut-open voltage clamp recordings of Na$^+$ currents from *Xenopus* oocytes expressing SkM1 α and $\beta1$ subunits. The membrane potential was stepped from -140 mV to potentials between -40 mV and -10 mV in 5-mV increments at 3-s intervals. (*B*) Cell-attached macropatch recordings from an oocyte expressing SkM1 α and $\beta1$ subunits. The membrane potential was stepped from -140 mV to potentials between -70 mV and -20 mV in 5-mV increments at 3-s intervals. (*C*) Cell-attached macropatch recordings from the SkM1 α subunit after completion of the time-dependent conversion to fast inactivation 15 min after formation of the seal. The membrane potential was stepped from -140 mV to potentials between -65 mV and -20 mV in 5-mV increments at 3-s intervals. (*D*) Current-voltage relationships comparing cut-open recording of $\alpha+\beta1$ subunits (*closed squares*, $n = 11$) to cell-attached macropatch recording of $\alpha+\beta1$ subunits (*closed circles*, $n = 9$), and to α subunit (*open circles*, $n = 10$) sodium current. (*E*) Steady-state inactivation curves for cut-open recording of $\alpha+\beta1$ subunits (*closed squares*, $n = 11$), cell-attached macropatch recording of $\alpha+\beta1$ subunits (*closed circles*, $n = 8$), and α subunit (*open circles*, $n = 9$) sodium current. Oocytes were held at -140 mV and depolarized, every 5 s, with an 800-ms conditioning pulse to produce inactivation. The peak current amplitude measured during a test pulse to the potential corresponding to peak inward current in *D* was normalized to the maximum current amplitude and was plotted as a function of the conditioning pulse potential. Both data sets were fit using the Boltzmann function yielding the indicated $V_{1/2}$ values. (*F*) The declining phase of the inward Na$^+$ current was fit with a single exponential function and corresponding mean ($\pm$SD) values of time constants were plotted as a function of membrane potential for oocytes expressing $\alpha+\beta1$ (cut-open, *closed squares*, $n = 11$), $\alpha+\beta1$ (macropatch, *closed circles*, $n = 9$) and α (macropatch, *open circles*, $n = 10$).
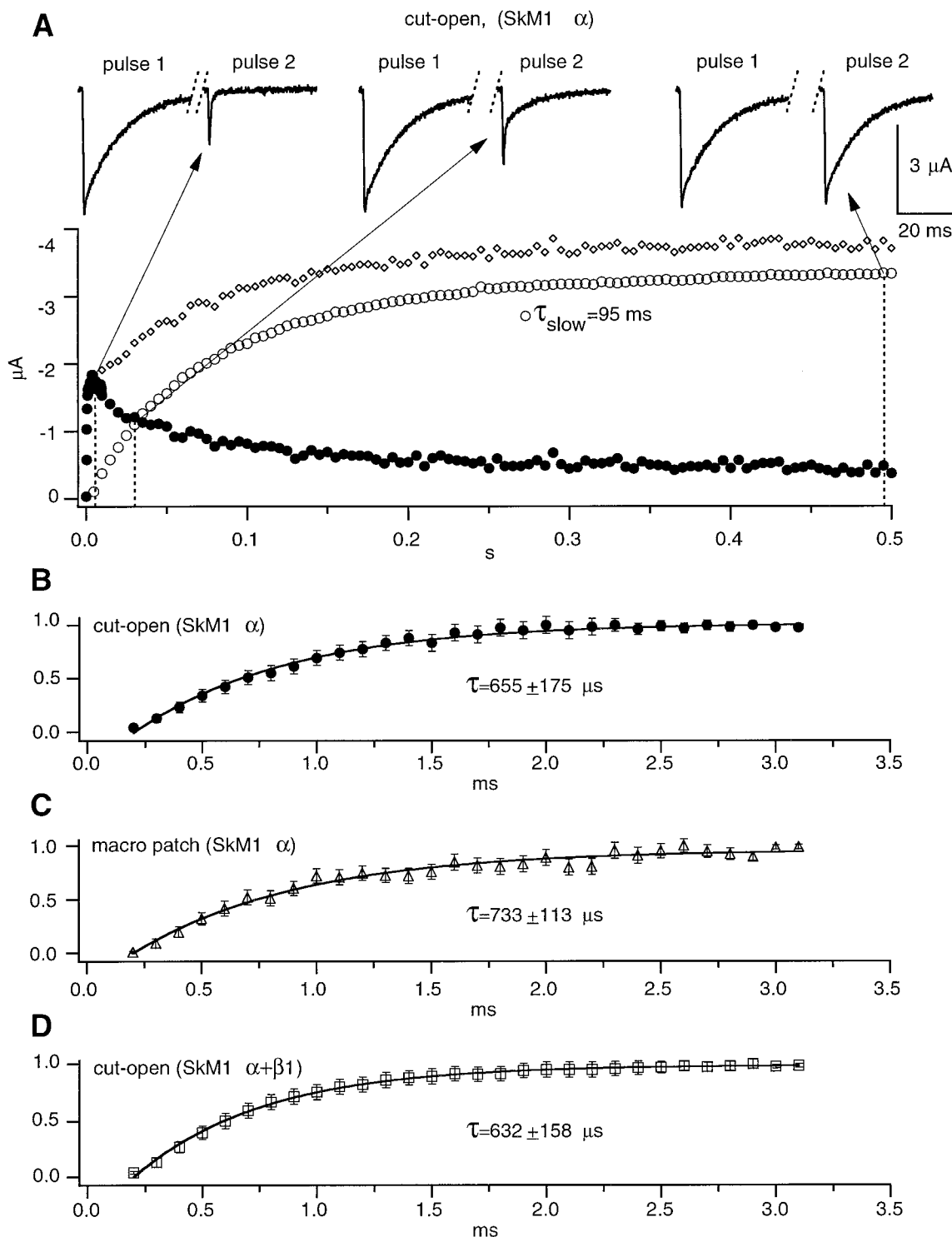
FIGURE 5 Time course of recovery from inactivation revealed interconversion between fast and slow inactivation modes. (*A*) Three sets of paired traces of SkM1 α subunit Na$^+$ current are shown with interpulse intervals corresponding to 0.003, 0.03, and 0.495 s. Both pulse 1 and 2 currents were elicited by 800-ms-long depolarizations from -140 mV to -10 mV, with 10-s recovery times between paired pulses (note that the traces shown were truncated). Pulse 2 current decay required fitting by the sum of two exponential curves with fast and slow time constants except for the briefest interpulse intervals. The amplitudes of fast (*closed circles*) and slow (*open circles*) components of pulse 2 current decay, estimated by the amplitudes predicted by each exponential component, are shown as a function of interpulse interval. Small diamonds represent the sum of fast and slow components of decay. (*B*) The recovery time course for the fast component of current decay shown in *A* on expanded time scale ($n = 5$). The points were fit by a single exponential curve yielding a fast recovery time constant of 655 ± 175 μs compared to the slow time constant of 94.6 ± 8.3 ms in *A*. (*C*) The corresponding recovery time course for the fast component of decay obtained by macropatch recording of the SkM1 α subunit ($n = 4$). (*D*) The recovery time course for the fast component of decay obtained by cut-open recording of the SkM1 $\alpha+\beta1$ subunit ($n = 4$).

inactivation in a manner similar to macropatch effects on the α subunit.

In contrast to the findings on inactivation kinetics, the effects of macropatch formation on the voltage-dependence of activation and steady-state inactivation were different from those mediated by the $\beta1$ subunit. Coexpression of the $\beta1$ subunit resulted in a small negative shift in the voltage-dependence of activation and inactivation measured using cut-open recordings (Figs. 1 and 2). The small shift by the $\beta1$ subunit contrasts with the large negative shift that accompanies the macropatch formation (Fig. 4). This large shift in voltage-dependence of activation and steady-state inactivation was not prevented by $\beta1$ coexpression (Fig. 4, D and E). Comparisons of macropatch recordings of $\alpha+\beta1$ current to α current revealed no significant difference.

Mechanical destabilization mediates the time-dependent shift to fast inactivation

A role of cytosolic factors in promoting a conversion to fast inactivation was indicated by our finding that the transition to fast gating was accelerated after patch excision. The idea that cytoskeleton might be involved was suggested by our finding that the conversion to fast gating was dependent on the size of the electrode tip. Micropatch recordings (electrode O.D. ~2–5 μm) showed little transition to fast inactivation over the time period that macropatch recordings exhibit conversion (Fig. 6, A and B). These micropatch recordings also failed to exhibit the negative shift in activation (Fig. 6 C) and steady-state inactivation (Fig. 6 D) that accompanies the formation of macropatches. The micropatch recordings were similar to those obtained from cut-open oocyte recordings in terms of both kinetics and voltage-dependence. Further similarities were also reflected in the somewhat slower activation kinetic when compared to macropatch recordings. Both micropatch (Fig. 6 B) and cut-open oocyte (Fig. 2 B) recorded current activated slower than macropatch inward current (Figs. 4 C and 6 A). It is not likely that these differences reflect inadequate voltage control because the differences can be observed for two different variations of cell-attached recording methods. Therefore, the faster rise of inward current observed with macropatch recording is likely to reflect accelerated activation, similar to the effects on inactivation. This macropatch-dependent speeding of activation kinetics may be, in part, responsible for the somewhat slower apparent inactivation rate measured for $\alpha+\beta1$ channels (Fig. 4 F). Thus, the more synchronized activation could provide for less overlap of activation and inactivation.

To examine for morphological changes that might accompany macropatch-induced, time-dependent changes in kinetics we utilized high-power differential interference contrast microscopy to examine the membrane within the macropatch pipette (Fig. 7). Simultaneous electrophysiological recordings monitored the change in kinetics of Na$^+$ current after formation of the seal. The video capture and

test depolarizations to activate maximal Na$^+$ current were synchronized at 5-s intervals. We found that the initial contact with the oocyte membrane dictated the amount of membrane that entered the electrode upon formation of a gigaohm seal. When the electrode was pressed firmly against the oocyte membrane, application of negative pressure resulted in the entry of a small dome of membrane. By contrast, when the macropatch electrode was allowed to lightly touch the oocyte membrane before application of negative pressure, a considerable amount of membrane entered the tip during application of negative pressure (Fig. 7). The latter method had the advantage that a large amount of pigmented cytoplasmic inclusions accompanied the membrane in the patch. As the membrane was slowly drawn in the electrode, these pigmented inclusions appeared to be drawn along by virtue of an apparent mechanical attachment to the membrane.

In a series of experiments ($n = 5$ cell attached patches) we controlled the pressure in the pipette interior to accelerate or prevent the growth of membrane area in the electrode (Fig. 8). Application of positive pressure (4–5 mmHg) prevented the increase in membrane area as well as conversion to fast inactivation. Alternatively, application of negative pressure facilitated the rate of conversion to fast inactivation. We took advantage of the observation that the rate of conversion could be accelerated by negative pressure to examine for morphological changes that might accompany conversion. The negative pressure was adjusted to speed conversion, and we observed a sudden change in morphology that accompanied the abrupt conversion to fast inactivation (Fig. 7). The pigmented inclusions, which were drawn toward the membrane as though attached, collapsed back into an amorphous ball at some critical degree of membrane stretch. The video frame showing this dissociation was precisely correlated with the abrupt change from slow to fast inactivation. Also, associated with the collapse in granule projections was a further increase in the swelling of the membrane in the pipette. Subsequent application of positive pressure to reduce the membrane area did not alter the inactivation or cause it to revert to slow inactivation. However, after the abrupt conversion to fast inactivation, a small non-inactivating component of inward current was observed. Release of negative pressure resulted in an immediate disappearance of this current (Fig. 7, *bottom right*) and reapplication of negative pressure resulted in reappearance. This inward current was likely due to the activation of stretch-activated ion channels that were associated with the expansion of the membrane. These findings were reliably reproduced on eight separate membrane patches, supporting the assertion that the detachment was causal to the change in inactivation kinetics.

Based on the observation that functional conversion was associated with disruption of cytoskeletal links to the membrane, we tested for a role of actin or microtubules in mediating the response. Inhibition of actin polymerization by treatment with 10 μM cytochalasin D ($n = 3$) (Cooper, 1987) or intracellularly injected 25 μg/oocyte at 5 U/mg
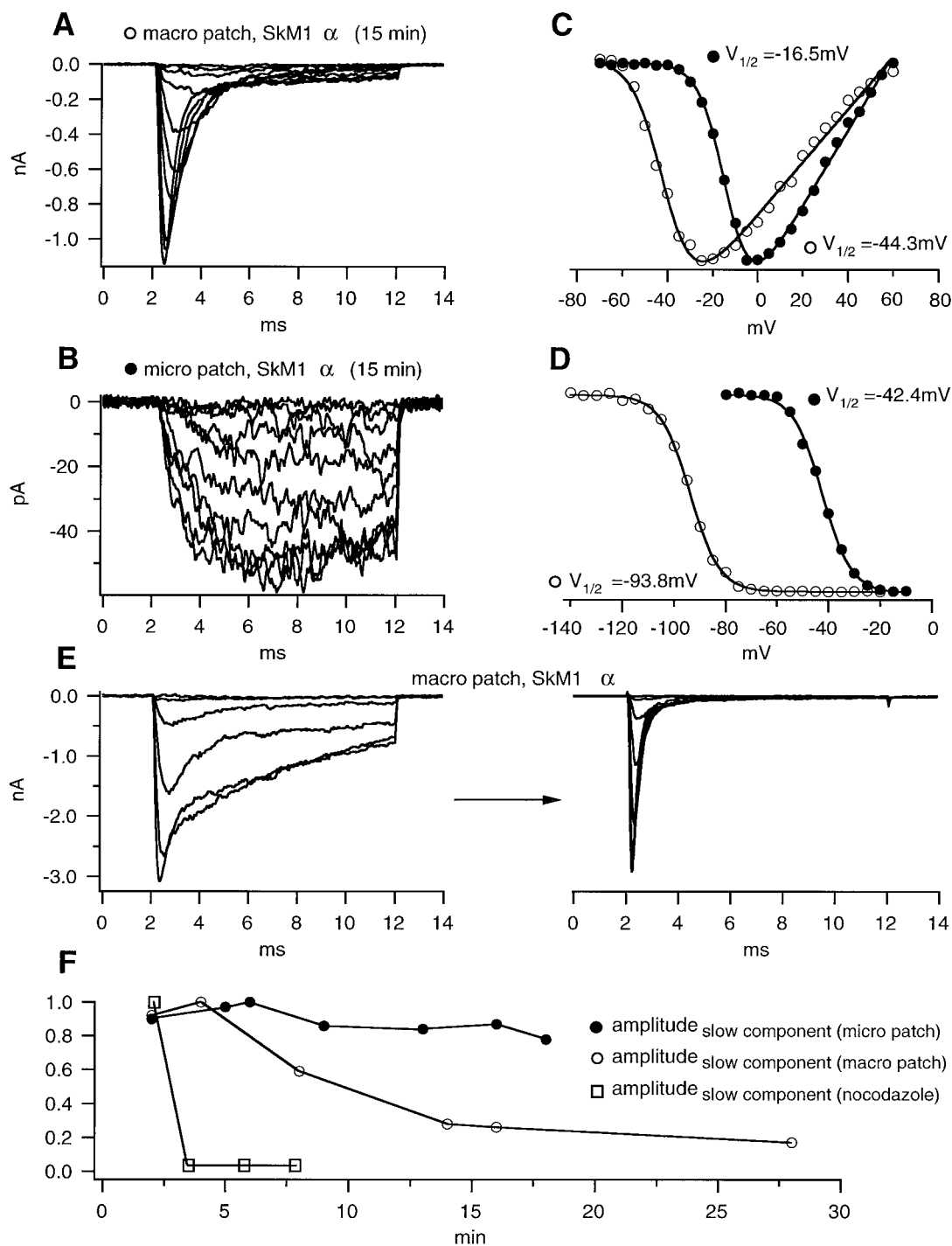
FIGURE 6 Effects of membrane patch size and microtubule disrupter, nocodazol, on time-dependent conversion to fast inactivation mode. (*A*) Macropatch recordings of Na$^+$ currents from oocytes expressing the SkM1 α subunit after a 15 min time-dependent conversion to fast inactivation. The membrane potential was stepped from -140 mV to potentials between -70 mV and -25 mV in 5-mV increments at 3-s intervals. (*B*) Micropatch (tip O.D. < 5 μm) SkM1 α subunit current recorded 15 min after seal formation. The membrane potential was stepped from -140 mV to potentials between -45 mV and 0 mV in 5-mV increments at 3-s intervals. (*C*) Current-voltage relationships comparing cell-attached macropatch (*open circles*) and micropatch (*closed circles*) recorded Na$^+$ current. (*D*) Steady-state inactivation curves for cell-attached macropatch (*open circles*) and micropatch (*closed circles*) recorded Na$^+$ current. Oocytes were held at -140 mV and depolarized, every 5 s, with an 800-ms conditioning pulse to produce inactivation. The peak current amplitude measured during a test pulse to the potential corresponding to peak inward current in *C* was normalized to the maximum current amplitude, and is plotted as a function of the conditioning pulse potential. Both data sets were fit using the Boltzmann function yielding the indicated $V_{1/2}$ values. (*E*) Representative macropatch recordings of SkM1 α subunit current immediately after seal formation and after an abrupt transition from predominantly slow to pure fast inactivation in oocytes after a 30-min treatment with 10 μM nocodazol at 4°C and an additional 3 h at room temperature. The membrane potential was held at -140 mV and stepped to potentials between -70 mV and -20 mV. (*F*) Comparisons of the time course of transition to fast inactivation for macropatch (*open circles*), micropatch (*closed circles*), and nocodazol-treated macropatch (*open squares*) sodium current. The amplitudes of fast and slow inactivating components were determined by the same approach described in Fig. 3.
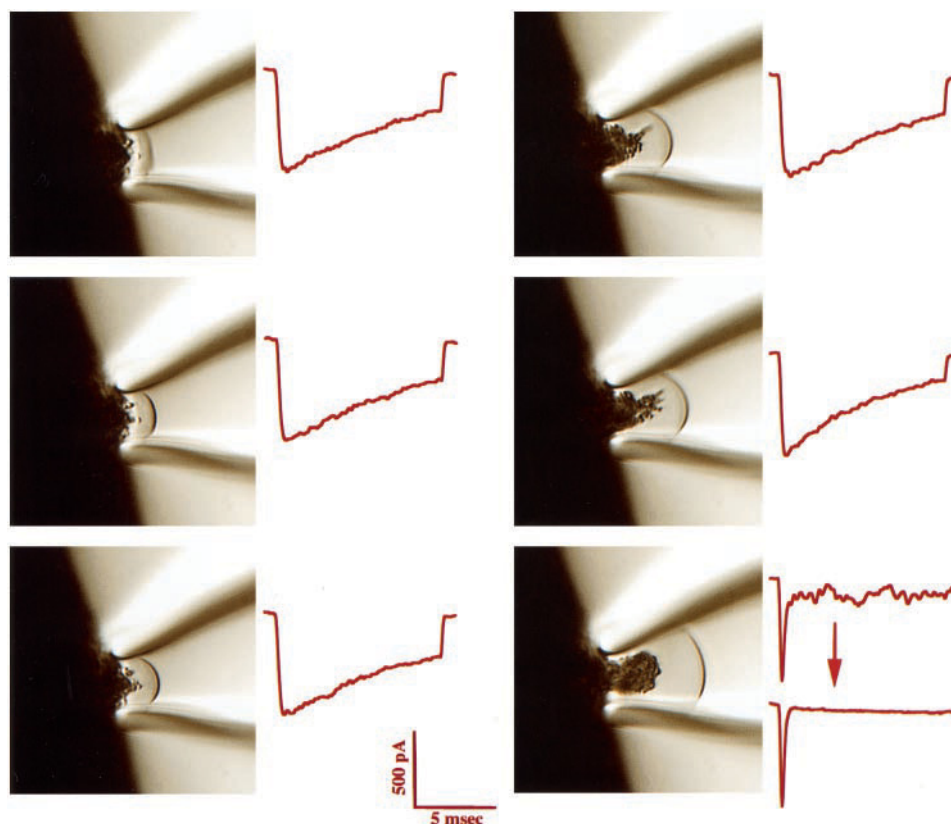
FIGURE 7   Collapse of membrane-attached cytoskeleton coincides with sudden transition to fast inactivation. Video sequence of macropatch membrane, acquired at 5-s intervals (*top to bottom*), showed time-dependent changes in membrane morphology in response to changes in intraelectrode pressure (electrode tip I.D. 10 μm). The first video frame (*top left*) corresponds to atmospheric pressure shortly after seal formation. During the subsequent video frames the pressure was decreased to -8 mmHg and the membrane was drawn into the electrode. Depolarizations from -100 mV to -10 mV were synchronized to the video capture. The associated SkM1 α subunit current exhibited slow inactivation during the first five video frames. Transition to fast inactivation occurred abruptly between the middle right and bottom right frames. The bottom right frame shows two traces; the top trace shows current recorded in the presence of negative pressure and the bottom trace follows release of pressure. During maintained negative pressure a stretch activated current was observed, which disappeared immediately upon release of the negative pressure. This stretch-activated current could be reactivated upon reapplication of negative pressure.

gelsolin ($n = 3$) (Kwiatkowski, 1999) resulted in a flattening of the oocyte. However, recordings of Na$^+$ current revealed no associated effects on channel kinetics or voltage-dependence. Intracellular injection of 10 μl 10 mM phalloidin ($n = 3$), an F-actin stabilizer (Cooper, 1987) also showed no effect on Na$^+$ channel function. In contrast, treatment with 10 μM nocodazol ($n = 3$), an inhibitor of microtubule polymerization (Hoebeke et al., 1976), affected the rate of conversion to fast inactivation. Instead of the gradual slow transition to fast inactivation, nocodazol-treated oocytes showed a complete and abrupt transition soon after formation of the macropatch (Fig. 6, *E* and *F*). Nocodazol had no effects on inactivation or voltage-dependence measured by cut-open recordings ($n = 6$). Several other widely used agents that interfere with microtubule formation, such as colcemide, colchicine, vincristine, and vinblastine, were without effect.

DISCUSSION

Our findings point to a dependence of voltage-activated Na$^+$ channel function on the type of methodology used to record Na$^+$ current. Specifically, macropatch recording of α subunit Na$^+$ current, in the absence of expressed auxiliary subunits, reveals large shifts in voltage-dependence and greatly accelerated inactivation (Fleig et al., 1994; Chen and Cannon, 1995) when compared to recordings made by either conventional microelectrode or cut-open oocyte methods. As discussed below, the regulation of function by recording configuration likely involves intermolecular interactions between the α subunit and cytoskeletal elements. The cytosolic regulation of α subunit function is reminiscent of regulation by the β1 subunit, suggesting the use of a common pathway.

The first functional consequence of the macropatch recording mode was a large negative shift in voltage-dependence of activation and inactivation of the α subunit Na$^+$ current compared to cut-open recordings. Both PN1 and SkM1 α subunits showed a 23-mV shift in the midpoint of peak activation and an even larger shift of 46 mV for steady-state inactivation, confirming previous macropatch studies on expressed α subunit channels in *Xenopus* oocytes (Fleig et al., 1994). This shift was fully established at the
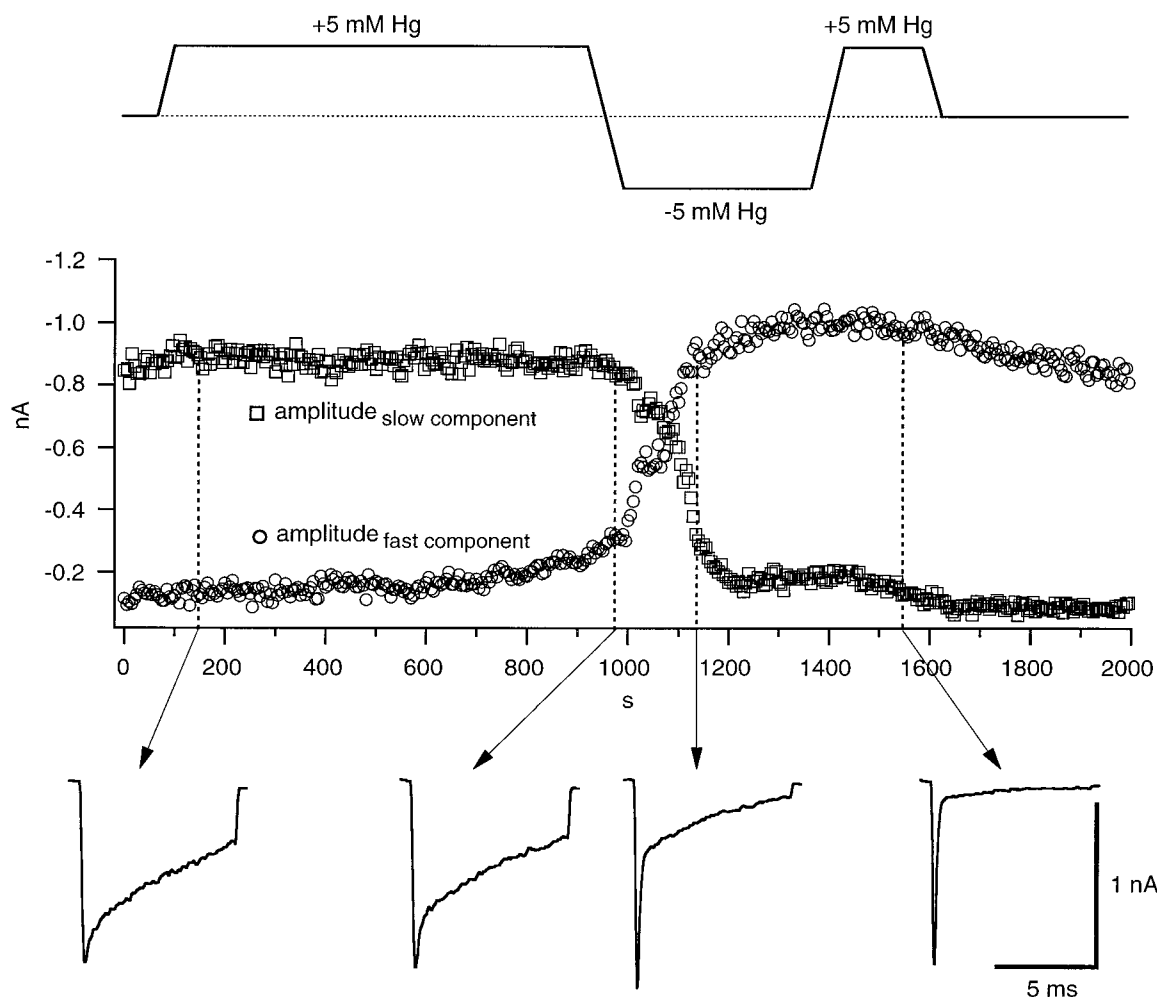
FIGURE 8   Pressure applied to the recording pipette interior regulates the rate of conversion to fast inactivation. Sample traces of SkM1 α subunit Na$^+$ currents evoked by voltage steps to -10 mV from a -100 mV holding potential and recorded by means of the cell-attached macropatch configuration. The decay phase of inward current was fit with a double exponential function, and corresponding amplitudes of fast (*open circles*) and slow (*open squares*) components were plotted as function of time (*middle panel*). The intrapipette pressure was regulated throughout the recording as depicted in the top panel. When the pressure was ramped from $+5$ mmHg to -5 mmHg an irreversible transition to fast inactivation was observed.

earliest measurable time following seal formation, thus setting it apart from the time-dependent shift in kinetics. Similar effects of patch formation on voltage-dependence of endogenous Na$^+$ current have been reported for chromaffin cells (Fenwick et al., 1982) and cardiac cells (Cachelin et al., 1983; Kunze et al., 1985; Kimitsuki et al., 1990). In an elegant study that combined two-microelectrode and cell-attached patch recordings of the same cell, a left shift in inactivation and activation was observed only for the patch current (Fahlke and Rudel, 1992). The lack of shift in microelectrode recorded current demonstrated that the gigaseal formation results in a local alteration in the functioning of the Na$^+$ channel. Interestingly, similar negative shifts have been associated commonly with ruptured whole-cell patch clamp recordings from native sodium currents (Fernandez et al., 1984; Wendt et al., 1992). Should such negatively shifted voltage-dependence exist for endogenous Na$^+$ current in mature neurons, the channels would be largely inactivated at resting membrane potential. This

raises the possibility that whole-cell patch clamp recording methods led to shifts in voltage-dependence similar to those mediated by patch formation, possibly through the same mechanism.

The second functional alteration that accompanied macropatch recordings was a time-dependent acceleration in inactivation kinetics, also confirming previous studies on expressed Na$^+$ channels (Fleig et al., 1994; Chen and Cannon, 1995). At the moment of seal formation and soon thereafter, the Na$^+$ current inactivated over tens of milliseconds. Typically, over time, the kinetics changed from slow inactivation, to mixed slow and fast inactivation, eventually displaying pure fast inactivation. This time-dependent change was observed for both neuronal (PN1) and skeletal muscle (SkM1) Na$^+$ channel isoforms (Figs. 1, *E* and *F*; 3, *B* and *C*). As with the shift in voltage-dependence, the effect of gigaseal formation on Na$^+$ current kinetics was local, as shown for studies on both native (Kunze et al., 1985; Kimitsuki et al., 1990) and expressed Na$^+$ current (Fahlke

and Rudel, 1992; Chen and Cannon, 1995). Single channel studies of rapidly and slowly inactivating components underlying macroscopic current have suggested that the SkM1 α subunit has intrinsic bimodal gating kinetics (Moorman et al., 1990; Zhou et al., 1991). The conversion was proposed to result from a time-dependent shift from a predominantly slow modal inactivation to a principally fast modal inactivation (Zhou et al., 1991). This idea is compatible with our findings for both PN1 and SkM1 Na^+ channels. First, our results show that during the transition to fast inactivation the decay of inward current was well-described by two individual components bearing fixed fast and slow decay rates, consistent with two modes. Second, we observed no change in peak current amplitude during the transition to fast inactivation; only the ratio of the fast and slow components changed. Finally, cut-open recordings indicated that slowly inactivating Na^+ current could be transiently and reversibly converted to fast inactivating current during repetitive depolarizations of the oocyte. This latter observation is best explained by differences in the rates of recovery from inactivation for fast and slow inactivating modes. It is unlikely that the shift in voltage-dependence was causal to or required for the eventual changes in inactivation kinetics. Cut-open recordings from oocytes injected with large amounts of SkM1 or PN1 RNA show substantial amounts of fast inactivation in the absence of a negative shift in voltage-dependence of activation and inactivation. Additionally, as mentioned above, upon repetitive stimulation, the slowly inactivating Na^+ current converted to purely fast inactivating Na^+ current (Krafte et al., 1990; Zhou et al., 1991; Fig. 5) without a negative shift in voltage-dependence.

The changes in voltage-dependence and inactivation kinetics may be the result of mechanical deformation associated with macropatch recording. For example, if small-diameter patch electrodes, instead of macropatch electrodes, were used to record Na^+ current, the time-dependent shift to fast inactivation was slowed and the negative shift in voltage-dependence was prevented. This reflects differences in the deformation of the membrane required to establish a gigaohm glass tissue seal. Direct evidence for the idea that deformation of a macropatch membrane leads to fast inactivation was provided by simultaneous imaging of patch membrane and electrophysiological recording of Na^+ current. Upon application of negative pressure to the patch membrane we observed an abrupt conversion from slow to fast inactivation at the exact moment of disruption of some type of attachment between the cell interior and the membrane. An expansion of the patch membrane within the electrode followed the rupturing of the attachments. While substantial alterations in membrane morphology are known to occur during patch formation (Milton and Caldwell, 1990; Sokabe and Sachs, 1990), our results provide the first direct evidence showing that disruption of cytoskeletal/membrane attachments mediates functional conversion of an ion channel. The question arises as to whether the conversion to fast inactivation is due to cytoskeletal disruption or to the resultant stretching of the membrane. For example,

changes in membrane tension (Opsahl and Webb, 1994; Lundbak et al., 1996) or membrane thickness (Haydon and Kimura, 1981; Hendry et al., 1985) have been shown to alter the voltage-dependence and/or inactivation kinetics of Na^+ channels. While it is clear that a critical level of stretch triggers the conversion, two observations support the idea that membrane tension per se is not the direct mediator of altered kinetics. First, after conversion by stretch, further distortions of the membrane elicited through application of negative or positive pressure had little or no effect on kinetics. In fact, the membrane could be reduced to its original area by means of positive pressure with no alteration in inactivation kinetics, showing the stretch per se has no effect. Second, reversible shifts to fast inactivation could be observed after repetitive depolarization using cut-open recording techniques: conditions that do not involve stretch.

It is also unlikely that the cytoplasmic attachments that were observed to break upon negative pressure were the direct mediators of functional conversion to fast inactivation, because patch excision did not lead to an abrupt change in kinetics. Instead, we propose that the additional membrane stretch, which occurred as a direct result of breaking these connections, altered a physical relationship between the α subunit and an associated structural protein(s). One site of interaction on the α subunit might govern the inactivation kinetics while a second, weaker interaction might affect the voltage-dependence. A "tethered" gating model (Hamill and McBride, 1997) postulated elastic coupling between cytoskeleton and gating structures on the channel, an idea that accounts for the key features associated with macropatch conversion of the α subunit. Ordinarily, such elastic interactions would provide for reversible transitions between slow and fast inactivation, like those observed during recovery of sodium current from the inactivated state. However, the dissolution of such elements following extreme stretch, as shown for macropatches (this article and Hamill and McBride, 1997) could result in irreversible conversion in both voltage-dependence and inactivation kinetics. The model would also potentially explain the observation that injection of large amounts of RNA encoding the α subunit led to significant amounts of fast inactivation (data not shown; Krafte et al., 1990; Zhou et al., 1991). In such oocytes the cytoskeletal proteins may be limiting and too few in number to provide for association with all of the α subunits.

Potential cytoskeletal candidates underlying the functional conversion continue to emerge from molecular studies of the α subunit and auxiliary proteins. Actin (Fukuda et al., 1981), syntrophin (Gee et al., 1998), and ankyrin (Srinivasan et al., 1988; Kordeli et al., 1990) have been shown to associate with the Na^+ channel α subunit. In our studies, disruption of actin had no effect on SkM1 Na^+ channel function. Functional studies have shown a dependence of squid axon Na^+ channel kinetics on microtubules (Matsumoto et al., 1984a, b). We observed an effect of nocodazol, an inhibitor of microtubule polymerization, on inactivation kinetics. Moreover, patches from nocodazol-treated oocytes

exhibited an abrupt shift in inactivation kinetics rather than the slow transition normally observed. We suspect that this reflects an indirect role of microtubules, such as countering membrane stretch, because nocodazol affected only the rate of macropatch-induced transition and exerted no effect on cut-open recordings of Na^+ current inactivation.

The macropatch-induced fast inactivation for the sodium α subunit alone represents a marked departure from the characteristically slow inactivation observed for cut-open recordings of α subunits. However, a striking similarity exists between the fast inactivation observed for these converted α subunits and for $\alpha+\beta1$ channels recorded by the cut-open technique. Both channel types recovered quickly from inactivation and good agreement was found for the time constants of recovery. Apparent small differences in kinetics were reflected in somewhat slower activation and inactivation of $\alpha+\beta1$ channels compared to macropatch-converted α subunits. Rather than representing actual differences in inactivation rates, it is likely that the faster decay was a direct consequence of faster and more synchronous activation for the macropatch-converted α subunit. Additional evidence for similarities between macropatch and $\beta1$ effects on α subunits was reflected in the absence of additive effects on the inactivation by the $\beta1$ subunit after macropatch conversion of the α subunit. The observed similarities between macropatch effects and $\beta1$ subunit-induced changes are important for two reasons. First, the functional conversion of the α subunit seen in macropatch recordings may help explain previously observed fast inactivation of Na^+ currents seen in the apparent absence of $\beta1$ subunits (Scheuer et al., 1990; Ukomadu et al., 1992; West et al., 1992; Chahine et al., 1994; Makita et al., 1994; Qu et al., 1994). Second, and more importantly, the similarities suggest a shared mechanism of action, raising the new possibility that the $\beta1$ subunit acts via interactions with the cytoskeleton. Accordingly, the $\beta1$ subunit might interfere with cytoskeletal components that normally bind to the α subunits. Such interference would cause mechanical destabilization, perhaps leading to a favoring of the intrinsic fast modal gating of the α subunit. Tests of this await identification of the specific regulatory molecules capable of binding to or modulating the α subunit.

REFERENCES

Auld, V. J., A. L. Goldin, D. S. Krafte, J. Marshall, J. M. Dunn, W. A. Catterall, H. A. Lester, N. Davidson, and R. J. Dunn. 1988. A rat brain Na^+ channel alpha subunit with novel gating properties. *Neuron.* 1:449–461.

Cachelin, A. B., J. E. De Peyer, S. Kokubun, and H. Reuter. 1983. Sodium channels in cultured cardiac cells. *J. Physiol. (Lond.).* 340:389–401.

Chahine, M., P. B. Bennett, A. L. George, Jr., and R. Horn. 1994. Functional expression and properties of the human skeletal muscle sodium channel. *Pflugers Arch.* 427:136–142.

Chen, C., and S. C. Cannon. 1995. Modulation of Na^+ channel inactivation by the β_1 subunit: a deletion analysis. *Pflugers Arch.* 431:186–195.

Cooper, J. A. 1987. Effects of cytochalasin and phalloidin on actin. *J. Cell Biol.* 105:1473–1478.

Fahlke, Ch., and R. Rudel. 1992. Giga-seal formation alters properties of sodium channels of human myobolls. *Pflugers Arch.* 420:248–254.

Featherstone, D. E., J. E. Richmond, and P. C. Ruben. 1996. Interaction between fast and slow inactivation in Skm1 sodium channels. *Biophys. J.* 71:3098–3109.

Fenwick, E. M., A. Marty, and E. Neher. 1982. Sodium and calcium channels in bovine chromaffin cells. *J. Physiol. (Lond.).* 331:599–635.

Fernandez, J. M., A. P. Fox, and S. Krasne. 1984. Membrane patches and whole-cell membranes: a comparison of electrical properties in rat clonal pituitary (GH_3) cells. *J. Physiol. (Lond.).* 356:565–585.

Fleig, A., P. C. Ruben, and M. D. Rayner. 1994. Kinetic mode switch of rat brain IIA Na channels in *Xenopus* oocytes excised macropatches. *Pflugers Arch.* 427:399–405.

Fukuda, J., M. Kameyama, and K. Yamaguchi. 1981. Breakdown of cytoskeletal filaments selectively reduces Na and Ca spikes in cultured mammal neurones. *Nature.* 294:82–85.

Gee, S. H., R. Madhavan, S. R. Levinson, J. H. Caldwell, R. Sealock, and S. C. Froehner. 1998. Interaction of muscle and brain sodium channels with multiple members of the syntrophin family of dystrophin-associated proteins. *J. Neurosci.* 18:128–137.

Goldin, A. L., T. Snutch, H. Lubbert, A. Dowsett, J. Marshall, V. Auld, W. Downey, L. C. Fritz, H. A. Lester, R. Dunn, W. A. Catterall, and N. Davidson. 1986. Messenger RNA coding for only the α subunit of the rat brain Na channel is sufficient for expression of functional channels in *Xenopus* oocytes. *Proc. Natl. Acad. Sci. USA.* 83:7503–7507.

Hamill, O. P., and D. W. McBride, Jr. 1997. Induced membrane hypo/hyper-mechanosensitivity: a limitation of patch-clamp recording. *Annu. Rev. Physiol.* 59:621–631.

Hartshorne, R. P., and W. A. Catterall. 1984. The sodium channel from rat brain: purification and subunit composition. *J. Biol. Chem.* 259:1667–1675.

Haydon, D. A., and J. E. Kimura. 1981. Some effects of n-pentane on the sodium and potassium currents of the squid giant axon. *J. Physiol. (Lond.).* 312:57–70.

Hendry, B. M., J. R. Elliott, and D. A. Haydon. 1985. Further evidence that membrane thickness influences voltage-gated sodium channels. *Biophys. J.* 47:841–845.

Hoebeke, J., G., Van Nijen, and M. De Brabander. 1976. Interaction of oncodazole (R 17934), a new antitumoral drug, with rat brain tubulin. *Biochem. Biophys. Res. Commun.* 69:319–324.

Isom, L. L., K. S. DeJongh, and W. A. Caterall. 1994. Auxiliary subunits of voltage-gated ion channels. *Neuron.* 12:1183–1194.

Isom, L. L., K. S. DeJongh, D. E. Patton, B. F. X. Reber, J. Offord, H. Charbonneau, K. Walsh, A. L. Goldin, and W. A. Catterall. 1992. Primary structure and functional expression of the β_1 subunit of the rat brain sodium channel. *Science.* 256:839–842.

Joho, R. H., J. R. Moorman, A. M. VanDongen, G. E. Kirsch, H. Silberberg, G. Schuster, and A. M. Brown. 1990. Toxin and kinetic profile of rat brain type III sodium channels expressed in *Xenopus* oocytes. *Brain Res. Mol. Brain Res.* 7:105–113.

Kimitsuki, T., T. Mitsuiye, and A. Noma. 1990. Negative shift of cardiac Na^+ channel kinetics in cell-attached patch recordings. *Am. J. Physiol.* 258:H247–H254.

Klugbauer, N., L. Lacinova, V. Flockerzi, and F. Hofmann. 1995. Structure and functional expression of a new member of the tetrodotoxin-sensitive voltage-activated sodium channel family from human neuroendocrine cells. *EMBO J.* 14:1084–1090.

Kordeli, E., J. Davis, B. Trapp, and V. Bennett. 1990. An isoform of ankyrin is localized at nodes of Ranvier in myelinated axons of central and peripheral nerves. *J. Cell Biol.* 110:1341–1352.

Krafte, D. S., A. L. Goldin, V. J. Auld, R. J. Dunn, N. Davidson, and H. A. Lester. 1990. Inactivation of cloned Na channels expressed in *Xenopus* oocytes. *J. Gen. Physiol.* 96:689–706.

Kunze, D. L., A. E. Lacerda, D. L. Wilson, and A. M. Brown. 1985. Cardiac Na currents and the inactivating, reopening, and waiting properties of single cardiac Na channels. *J. Gen. Physiol.* 86:691–719.

Kwiatkowski, D. J. 1999. Function of gelsolin: motility, signaling, apoptosis, cancer. *Curr. Opin. Cell Biol.* 11:103–108.

Leonard, J., T. Snutch, H. Lubbert, N. Davidson, and H. A. Lester. 1986. Macroscopic Na currents with gigaohm seals on mRNA-injected *Xenopus* oocytes. *Biophys. J.* 49:386*a*. (Abstr.).

Lundbak, J. A., P. Birn, J. Girshman, A. J. Hansen, and O. S. Andersen. 1996. Membrane stiffness and channel function. *Biochemistry.* 35:3825–3830.

Makita, N., P. B. Bennet, Jr., and A. L. George, Jr. 1994. Voltage-gated Na$^+$ channel β1 subunit mRNA expressed in adult skeletal muscle, heart, and brain is encoded by a single gene. *J. Biol. Chem.* 269:7571–7578.

Matsumoto, G., M. Ichikawa, and A. Tasaki. 1984a. Axonal microtubules necessary for generation of sodium current in squid giant axons. II. Effect of colchicine upon asymmetrical displacement current. *J. Membr. Biol.* 77:93–99.

Matsumoto, G., M. Ichikawa, A. Tasaki, H. Murofushi, and H. Sakai. 1984b. Axonal microtubules necessary for generation of sodium current in squid giant axons. I. Pharmacological study on sodium current and restoration of sodium current by microtubule proteins and 260K protein. *J. Membr. Biol.* 77:77–91.

Milton, R. L., and J. H. Caldwell. 1990. Na current in membrane blebs: implications for channel mobility and patch clamp recording. *J. Neurosci.* 10:885–893.

Moorman, J. R., G. E. Kirsch, A. M. VanDongen, R. H. Joho, and A. M. Brown. 1990. Fast and slow gating of sodium channels encoded by a single mRNA. *Neuron.* 4:243–252.

Murray, N., Y-C. Zheng, G. Mandel, P. Brehm, R. Bolinger, Q. Reuer, and R. Kullberg. 1995. A single site on the ϵ subunit is responsible for the change in Ach receptor channel conductance during skeletal muscle development. *Neuron.* 14:865–870.

Opsahl, L. R., and W. W. Webb. 1994. Transduction of membrane tension by the ion channel alamethicin. *Biophys. J.* 66:71–74.

Qu, Y., J. Rogers, T. Tanada, T. Scheuer, and W. A. Catterall. 1994. Modulation of cardiac Na$^+$ channels expressed in a mammalian cell line and in ventricular myocytes by protein kinase C. *Proc. Natl. Acad. Sci. USA.* 91:3289–3293.

Rudy, B. 1978. Slow inactivation of the sodium conductance in squid giant axons. Pronase resistance. *J. Physiol. (Lond.).* 283:1–21.

Scheuer, T., V. J. Auld, S. Boyd, J. Offord, R. Dunn, and W. A. Catterall. 1990. Functional properties of rat brain sodium channels expressed in a somatic cell line. *Science.* 247:854–858.

Sokabe, M., and F. Sachs. 1990. The structure and dynamics of patch-clamped membranes: a study using differential interference contrast light microscopy. *J. Cell Biol.* 111:599–606.

Srinivasan, Y., L. Elmer, J. Davis, V. Bennet, and K. Angelides. 1988. Ankyrin and spectrin associate with voltage-dependent sodium channels in brain. *Nature.* 333:177–180.

Taglialatela, M., L. Toro, and E. Stefani. 1992. Novel voltage clamp to record small, fast currents from ion channels expressed in *Xenopus* oocytes. *Biophys. J.* 61:78–82.

Townsend, C., and R. Horn. 1997. Effect of alkali metal cations on slow inactivation of cardiac Na$^+$ channels. *J. Gen. Physiol.* 110:23–33.

Trimmer, J. S., S. S. Cooperman, S. A. Tomiko, J. Zhou, S. M. Crean, M. B. Boyle, R. G. Kallen, Z. Sheng, R. L. Barchi, F. J. Sigworth, R. H. Goodman, W. S. Agnew, and G. Mandel. 1989. Primary structure and functional expression of a mammalian skeletal muscle sodium channel. *Neuron.* 3:33–49.

Ukomadu, C., J. Zhou, F. J. Sigworth, and W. S. Agnew. 1992. μ1 Na$^+$ channels expressed transiently in human embryonic kidney cells: biochemical and biophysical properties. *Neuron.* 8:663–676.

Vedantham, V., and S. C. Cannon. 1998. Slow inactivation does not affect movement of the fast inactivation gate in voltage-gated Na$^+$ channels. *J. Gen. Physiol.* 111:83–93.

Wendt, D. J., C. F. Starmer, and A. O. Grant. 1992. Na channel kinetics remain stable during perforated-patch recordings. *Am. J. Physiol.* 263:C1234–C1240.

West, J. W., T. Scheuer, L. Maechler, and W. Catterall. 1992. Efficient expression of rat brain type IIA Na$^+$ channel α subunits in a somatic cell line. *Neuron.* 8:59–70.

Zhou, J. Y., J. F. Potts, J. S. Trimmer, W. S. Agnew, and F. J. Sigworth. 1991. Multiple gating modes and the effect of modulating factors on the μI sodium channel. *Neuron.* 7:775–785.